ADVANCED POWER ELECTRONICS INTERFACE FOR SEIG BASED WIND POWER GENERATION WITH BATTERY ENERGY BACK UP UNIT WITH GRID INTERACTION

[1]KRISHNA RAKESH KHANNAN, [2]B.SH SURESH KUMAR

[1]Student, [2]Assistant Professor
Gokul Institute of Technology & Sciences, Bobbili, Andhra Pradesh, India

Abstract- Present energy need heavily relies on the conventional sources. But the limited availability and steady increase in the price of conventional sources has shifted the focus toward renewable sources of energy. Of the available alternative sources of energy, wind energy is considered to be one of the proven technologies. With a competitive cost for electricity generation, wind energy conversion system (WECS) is nowadays deployed for meeting both grid-connected and stand-alone load demands. However, wind flow by nature is intermittent. In order to ensure continuous supply of power suitable storage technology is used as backup. In this work, the sustainability of a 4-kW hybrid of wind and battery system is investigated for meeting the requirements of a 3-kW stand-alone dc load representing a base telecom station. A charge controller for battery bank based on turbine maximum power point tracking and battery state of charge is developed to ensure controlled charging and discharging of battery. The mechanical safety of the WECS is assured by means of pitch control technique. Both the control schemes are integrated and the efficacy is validated by testing it with various load and wind profiles in MATLAB/SIMULNIK.

Later, this project is extended towards grid integration using advanced power electronics along with better control strategies for voltage regulation and load sharing. Field oriented stationary current controller used for the purpose of current controller and dc bus regulation method is used to maintain the dc bus voltage constant there by maintained inverter output voltage of required to meet the voltage regulation limits. Simulation based results demonstrates that proposed controllers along with advance power electronics schemes successfully used for the mentioned purpose

I. INTRODUCTION

The proposed hybrid system comprises of a 4-kWWECS and 400 Ah, C/10 lead acid battery bank. The system is designed for a 3-kW stand-alone dc load. The layout of the entire system along with the control strategy is shown in Fig.2. The specifications of the WT, SEIG, and battery bank are tabulated. The WECS consists of a 2.2-kW horizontal axis WT, gear box with a gear ratio of 1:8 and a 5.4 hp SEIG as the WTG. Since the load is a stand-alone dc load the stator terminals of the SEIG are connected to a capacitor bank for self-excitation. The ac output is rectified by three-phase uncontrolled diode rectifier. However, there is a need for a battery backup to meet the load demand during the period of unavailability of sufficient wind power. This hybrid wind-battery system requires suitable control logic for interfacing with the load. The uncontrolled dc output of the rectifier is applied to the charge controller circuit of the battery. The charge controller is a dc–dc buck converter which determines the charging and discharging rate of the battery. The battery bank connected to the system can either act as a source or load depending on whether it is charging or discharging. However, regardless of this the battery ensures that the load terminal voltage is regulated. Further, as shown in Fig. 1, the charging of the battery bank is achieved by MPPT logic, while the pitch controller limits the mechanical and electrical parameters within the rated value. The integrated action of the battery charge and pitch controller ensures reliable operation of the stand-alone WECS.

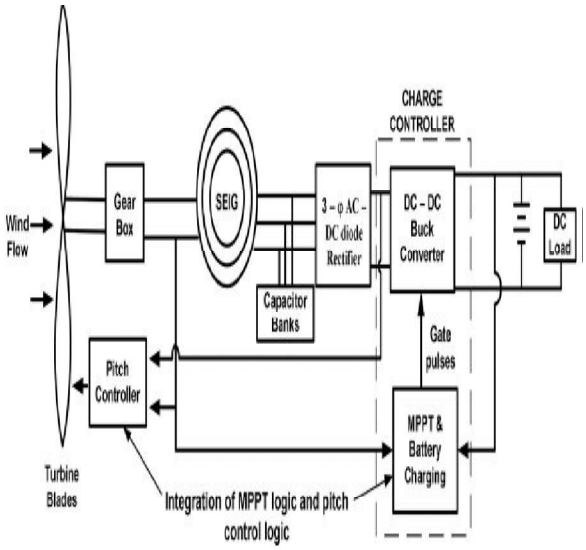

Figure 1 Layout of hybrid wind–battery system for a stand-alone dc load.

II. PROPOSED SYSTEM

2.2 CONTROL STRATEGY FOR STAND-ALONE HYBRID WIND-BATTERY SYSTEM

The wind flow is erratic in nature. Therefore, a WECS is integrated with the load by means of an ac–dc–dc converter to avoid voltage flicker and harmonic generation. The control scheme for a stand-alone hybrid wind-battery system includes the charge controller circuit for battery banks and pitch control logic to ensure WT operation within the rated value. The control logic ensures effective control of the WECS against all possible disturbances.

2.2.1 Charge Controller for the Battery Bank

This section discusses in detail the development of charge controller circuit for a 400 Ah, C/10 battery bank using a dc–dc buck converter in MATLAB/SIMULINK platform. Generally, the batteries are charged at C/20, C/10, or C/5 rates depending on the manufacturer's specification where C specifies the Ah rating of battery banks. So, the battery bank system considered in the design can be charged at 20, 40, or 80 A. But, in this work C/10 rate (i.e., 40 A) for battery charging is chosen. However, the current required for charging the battery bank depends on the battery SOC. A typical battery generally charges at a constant current (CC), i.e., C/10 rate mode till battery SOC reaches a certain level (90%–98%). This is referred to as CC mode of battery charging. The CC mode charges the battery as fast as possible. Beyond this SOC, the battery is charged at a constant voltage (CV) which is denoted as CV mode of battery charging in order to maintain the battery terminal voltage.

2.2.2 Control Strategy

The implementation of the charge control logic as shown in Fig. 2.3 is carried out by three nested control loops. The outer most control loop operates the turbine following MPPT logic with battery SOC limit. To implement the MPPT logic, the actual tip speed ratio (TSR) of turbine is compared with the optimum value. The error is tuned by a PI controller to generate the battery current demand as long as the battery SOC is below the CC mode limit. Beyond this point, the SOC control logic tries to maintain constant battery charging voltage. This in turn reduces the battery current demand and thus prevents the battery bank from overcharging. The buck converter inductor current command is generated in the intermediate control loop. To design the controller, it is essential to model the response of the battery current (*Ib*) with respect to the inductor current (*IL*). The transfer function can be computed from Fig. 2.2and is given by

$$\frac{I_b(s)}{I_L(s)} = \frac{r_c C s + 1}{LCs^2 + (r_L + r_c + r_b) Cs + 1}.$$

As shown in Fig.2.2, the battery is assumed to be a CV source with a small internal resistance (*rb*). The effective series resistances (ESR) of the capacitor (*rc*) and the inductor (*rL*) are also considered. The ESR of the capacitor and the inductor is taken o be 1mΩ each. The battery internal resistance is 10 mΩ. For regulating the peak-to-peak (p–p) ripple of battery current and converter output voltage within 2% of the rated value the L and C are calculated to be 10 mH and 5 mF, respectively. For controlling the battery current the actual converter output current (*Id*) is compared with the reference (*Ib* + *Ia*) and the error is processed by a cascade of a PI and a lead compensator. The PI controller is modelled as an inverted zero.

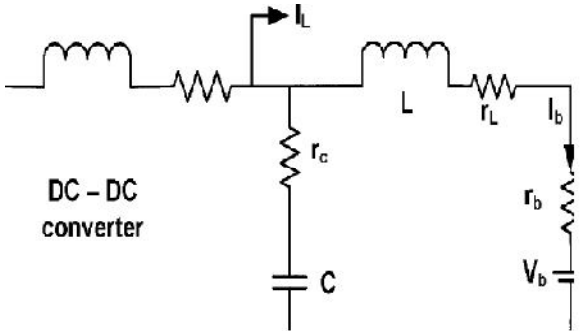

Figure 2.2 Circuit representation of buck converter output.

To maintain the phase margin of the open-loop system the frequency of this zero is 50 times lower than the crossover frequency. To improve the phase margin of the battery charging current control loop (i.e., (1) along with the PI controller) a lead compensator is connected in cascade with the PI controller as shown in Fig. 2. The output of the lead compensator determines inductor current reference for the dc–dc converter. In order to prevent over loading the turbine (and its consequent stalling) the lead compensator output is first passed through an adjustable current limiter. The lower limit is set to zero and the upper limit is varied according to the maximum power available at a given wind speed. The output of this limiter is used as the reference for the current controller in the dc–dc converter. Finally, in the inner most loop the actual inductor current is made to track the reference using peak current mode control. The compensated output of the intermediate loop is compared with the instantaneous inductor current of the buck converter. The output of the comparator is applied to an SR flipflop to produce the gate pulses for the dc–dc buck converter. The frequency of the clock pulses is 2 kHz. The frequency of the gate pulse is equal to the clock pulse frequency. This method of generating gate pulses for the converter is known as the current programmed control technique. The advantage of this method is that it does not allow the inductor current to go beyond the rated limit. This in turn protects the buck converter switch and inductor from over current situation.

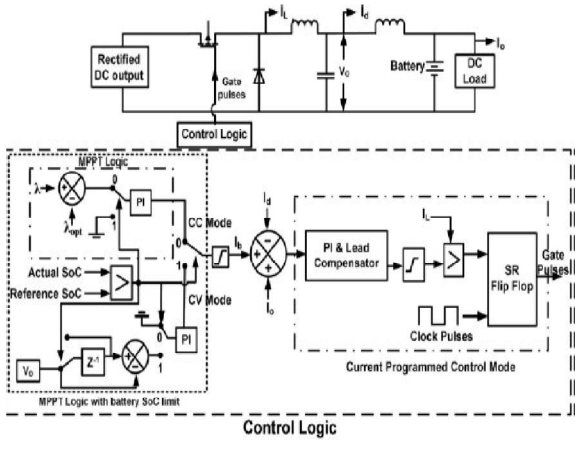

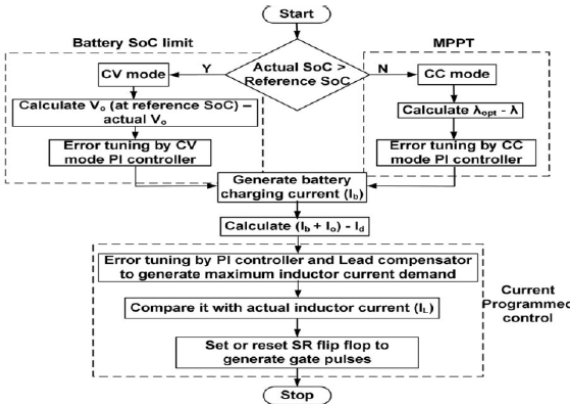

Figure 2.3 schematic block and flowchart of the charge controller circuit for battery.

2.3 MODES OF BATTERY CHARGING

2.3.1 CC Mode of Battery Charging

In CC mode, the battery charging current demand is determined from the MPPT logic. MPPT is implemented by comparing the actual and optimum TSR (λopt). The error is tuned by a PI controller to generate the battery charging current as per the wind speed. In this mode, the converter output voltage rises with time while the MPPT logic tries to transfer as much power as possible to charge the batteries. The actual battery charging current that can be achieved does not remain constant but varies with available wind speed subject to a maximum of C/10 rating of the battery. The battery charging current command has a minimum limit of zero. In case the wind speed is insufficient to supply the load even with zero battery charging current the inductor current reference is frozen at that particular value and the balance load current is supplied by the battery.

2.3.2 CV Mode of Battery Charging

In the CC mode, the battery voltage and SoC rise fast with time. However, the charge controller should not overcharge the batteries to avoid gasification of electrolyte. As a result, once the battery SoC becomes equal to the reference SoC the controller must switch over from CC mode to CV mode. In CV mode, the battery charging voltage is determined from the buck converter output voltage (Vo). The value of the converter voltage when the battery SoC reaches 98% is set as the reference value and is compared with the actual converter output voltage. The error in the voltage is then controlled by a cascaded arrangement of PI controller and lead compensator to generate the inductor current reference. It is then compared with the actual inductor current by a logical comparator to generate gate pulses in a similar way as described in Section A. In this mode, the converter output voltage is maintained at a constant value by the controller action. So, in CV mode the battery voltage and SoC rise very slowly with time as compared to CC mode. The battery charging current slowly decreases with time, since the potential difference between the buck converter output and battery terminal gradually reduces. Thus, in CC mode the buck converter output current is regulated while the output voltage keeps on increasing with time. On the contrary in CV mode the output voltage is regulated, while the current in the circuit reduces gradually. To study the CC and CV mode of battery charging, rated value of wind speed is applied to the system. The battery parameters and the converter output parameters are observed with time. The results are shown in Fig. 2.2.

As shown in Fig. 2.4, the battery is charged both in CC mode and CV mode. The transition from CC to CV mode takes place when the battery SoC reaches 98%. This is because in the present design, the threshold SoC for switch over in the control logic is set at 98%. As discussed in the earlier section, in the CC mode the battery charges at a CC of 40 A which is the C/10 value for a 400-Ah battery bank. During this mode, both converter output voltage and battery voltage rise. The battery SoC rises from an initial SoC level of 97.95% to 98% within 17 s. As the battery reaches the threshold SoC level, the buck converter voltage is regulated by the controller action at a constant value of 53 V while the converter current gradually reduces from 40 A at 17 s to 10 A at 40 s. The battery SoC slowly rises from 98% to 98.03%. The results indicate that the battery charges at a faster rate in CC mode as compared to CV mode. Thus, in CC mode much of the available power from primary source is injected into the battery whereas in CV mode the battery is charged slowly to avoid gasification and heating issue.

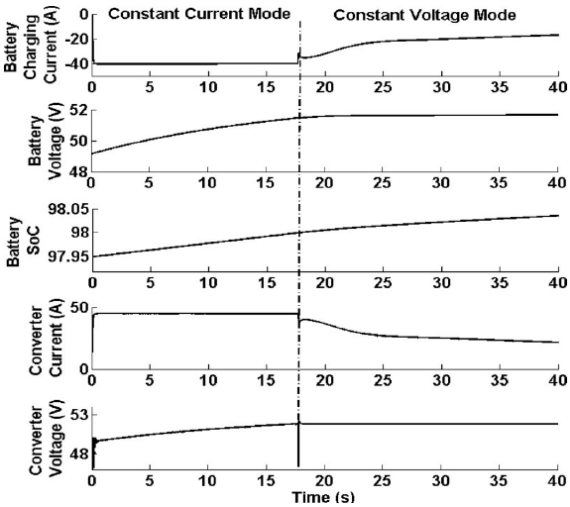

Figure 2.4 Battery charging modes at a constant wind speed of 10 m/s.

2.4 PITCH CONTROL MECHANISM

The WT power output is proportional to the cube of wind velocity. generally the cut-off wind speed of a modern WT is much higher compared to the rated wind speed. If the WT is allowed to operate over the entire range of wind speed without implementation of any control mechanism, the angular speed of the shaft exceeds its rated value which may lead to damage of

the blades. So, it is very much essential to control the speed and power at wind speeds above the rated wind speed. This is achieved by changing the pitch angle of the blade. Such a mechanism is referred to as the pitch control of WT. The power coefficient (Cp) versus TSR (λ) characteristics of the WT considered in this study for different pitch angles are shown in Fig. 2.6. As examined from the characteristics, at a pitch angle of zero degree the value of Cp is maxima. But the optimum value of power coefficient reduces with increase in pitch angle. This happens because with increase in blade pitch the lift coefficient reduces which results in decreasing the value of Cp. So, the pitch control mechanism controls the power output by reducing the power coefficient at higher wind speeds. Below the rated wind speed the blade pitch is maintained at zero degree to obtain maximum power. The pitch controller increases the blade pitch as the WT parameters exceed the rated value. The reduction in the value of Cp by pitching compensates for the increase in WT power output under the influence of higher wind speeds. Apart from regulating the WT parameters, it is also essential to control the output voltage of the ac–dc rectifier to avoid overvoltage condition in the WECS. Hence, the pitch controller ensures that with desirable pitch command, the WT parameters and the rectifier output dc voltage are regulated within their respective maximum allowable limits to ensure safe operation of the WECS.

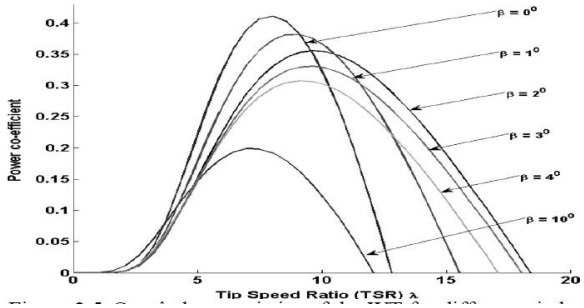

Figure 2.5 $Cp - \lambda$ characteristics of the WT for different pitch angles.

2.5 PITCH CONTROL SCHEME

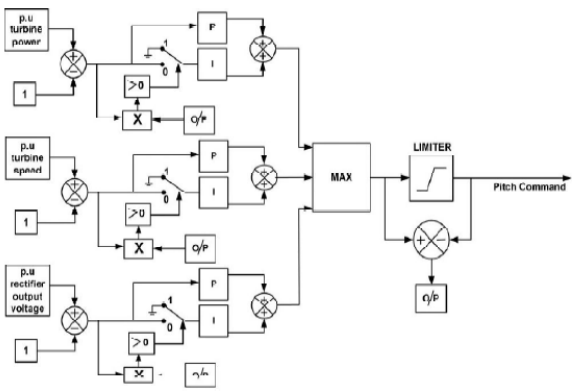

Figure 2.6 Control Scheme of Pitch angle control

The pitch control scheme is shown in Fig. 2.6. As seen the p.u. value of each input is compared with 1 to calculate the error. The errors are tuned by PI controller. The "MAX" block chooses the maximum output from each PI controller which is then passed on to a limiter to generate the pitch command for the WT. The actual pitch command is compared with the limited value. The lower limit of the pitch command is set at zero. There arises an error when the actual pitch command goes above or below the specified limit. This is multiplied with the error obtained from each of the comparator. The product is compared with zero to determine the switching logic for integrator. This technique is carried out to avoid integrator saturation. The pitch controller changes the pitch command owing to variation in turbine rotation speed, power, and output voltage of rectifier, which ensures safe operation of the WECS.

2.6 *GENERATOR* SIDE CONVERTER CONTROL TECHNIQUE

The objectives of the machine ($SCIG_w$) side converter are to achieve optimum torque for MPT for $SCIG_w$ and to provide the required magnetizing current to the $SCIG_w$.

2.6.1 Speed-Control Loop for MPT

In the proposed algorithm, the rotor position (θ_{rw}) of SCIGw and the wind speed are sensed. The rotor speed (ω_{rw})of SCIGw is determined from its rotor position (θ_{rw}). The tip speed ratio (λ_w) for a wind turbine of radius (r_w) and gear ratio (η_w) at a wind speed of $v_w$is defined as

$$\lambda_w = \frac{\omega_{rw}\, r_w}{\eta_w\, v_w}$$

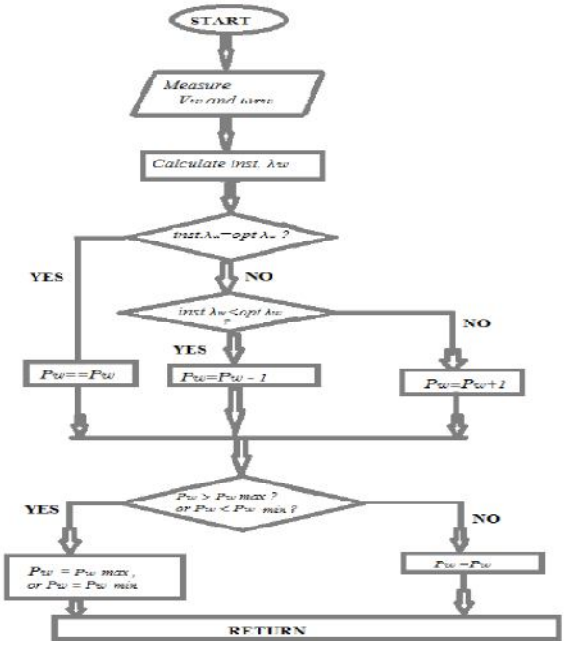

Figure 2.7. Flow chart diagram of MPT technique.

For MPT in the wind-turbine-generator system, the $SCIG_w$ should operate at the optimum tip speed ratio

(λ_w^*) Thus the reference rotor speed (w_{rw}^*) for MPT is generated using equation as

$$\lambda_w^* = \frac{\omega * rw\, r_w}{\eta_w\, v_w}$$

The flow chart diagram for the proposed MPT technique is given in Fig.2.7

2.6.2 Reference q-axis $SCIG_w$ Stator-Current Generation

The reference rotor speed of $SCIG_w$ is compared with (ω_{rw})to calculate the rotor-speed error (ω_{rwer}) at the n^{th} sampling instant as

$$\omega_{rwer(n)} = \omega_{rw(n)}^* - \omega_{rw(n)}^*$$

The aforementioned error is fed to the speed proportional integral (PI) controller. At the n^{th}sampling instant, the output of the speed PI controller with proportional gain $K_{p\omega}$and integral gain $K_{i\omega}$ gives the reference *q*-axis $SCIG_w$ stator current (I_{qsw}^*).

2.6.3. Reference d-axis $SCIG_w$ Stator-Current Generation

The reference *d*-axis $SCIG_w$ stator current (I_{dsw}^*) is determined from the rotor flux set point ($\varphi^*{}_{drw}$) at the n^{th} sampling instant as [23]

$$I_{dsw(n)}^* = \frac{\varphi_{drw}^*}{L_{mw}}$$

Where L_{mw} is the magnetizing inductance of $SCIG_w$

C. Generation of PWM Signal for Machine-Side Converter:

For generation of three-phase reference $SCIG_w$ stator currents (i_{swa}^*, i_{swb}^* , andi_{swc}^*), the transformation angle $\theta_{rotorflux\,w}$ is[25]

$$\theta_{rotor\ flux\ w} = \theta_{slip\,w} + \left(\frac{pw}{2}\right)\theta_{rw}$$

The references for d-q components of $SCIG_w$stator currents are converted as

$$i_{swa}^* = I_{dsw}^* \sin(\theta_{rotor\ flux\ w}) + I_{qsw}^* \cos(\theta_{rotor\ flux\ w})$$

$$i_{swb}^* = I_{dsw}^* \sin(\theta_{rotor\ flux\ w} - 2\pi/3) + I_{qsw}^* \cos(\theta_{rotor\ flux\ w} - 2\pi/3)$$

$$i_{swc}^* = I_{dsw}^* \sin(\theta_{rotor\ flux\ w} + 2\pi/3) + I_{qsw}^* \cos(\theta_{rotor\ flux\ w} + 2\pi/3)$$

The three-phase reference $SCIG_w$ stator currents (i_{swa}^*, i_{swb}^* , and i_{swb}^*) are then compared with the sensed $SCIG_w$ stator currents (i_{swa} , i_{swb} and i_{swc})to compute the SCIG*w* stator current errors, and these current errors are amplified with gain (*K* = 5) and the amplified signals are compared with a fixed frequency (10 kHz) triangular carrier wave of unity amplitude to generate gating signals for the IGBTs of the machine-side VSC. The sampling time of the controller is taken as 50 *μs*, as this time is sufficient for completion of calculations in a typical DSP controller. The total control mechanism of machine side converter is shown in Fig.2.8.

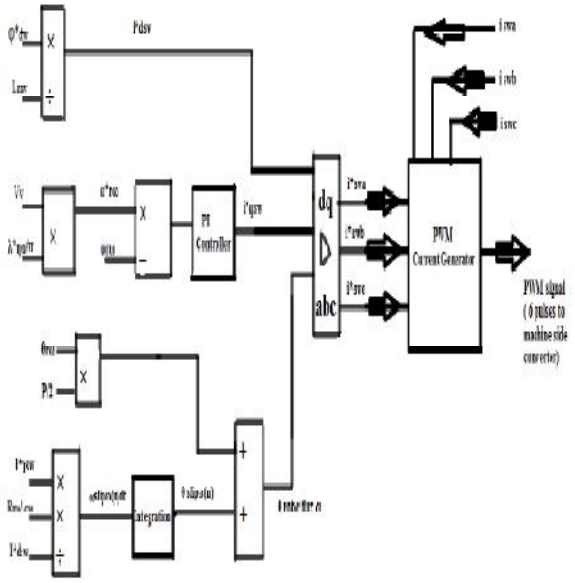

Figure 2.8 Control Scheme of Machine side converter.

III. SIMULINK CIRCUITS AND RESULTS

The wind energy conversion system is validated by computer simulation, using Matlab PowerSym toolbox. The WT model is obtained from equation (1) and from an approximation of the CP curve in terms of the tip speed ratio (L). Therefore, input signals for the WT model are the wind speed and system rotor speed. The gearbox was modeled as a gain for simplicity reasons. The PMSG was chosen from the PowerSym preset generators list. With the goal of a correct observation and analysis of the proposed power and control systems behavior, the wind was supposed as a known and controllable parameter. The proposed wind energy conversion system was verified by simulation for a standalone application. System parameters are shown in Table 2. Results of the rotor speed control are shown in Figures 7 and 8. Figure 7 shows the rotor speed behavior for successive raising steps of wind speed (3 m/s to 4 m/s then 5 m/s). Figure 8 shows the down steps. Electric variables are shown for the same cases in Figures 9 and 10. From Figures 7 and 8 it can be observed that the proposed control system (decoupled linear speed control plus feedforward converters control) can follow correctly the speed reference. A less than 20% overstep is observed when the wind speed step rises; nevertheless, when the wind speed step goes down, the obtained overstep is much higher, near 50 %. Some small oscillations are observed in steady state also. These effects can be corrected by adjusting the controller parameters and can be explained by non linear and high frequency dynamics that are neglected by the control system

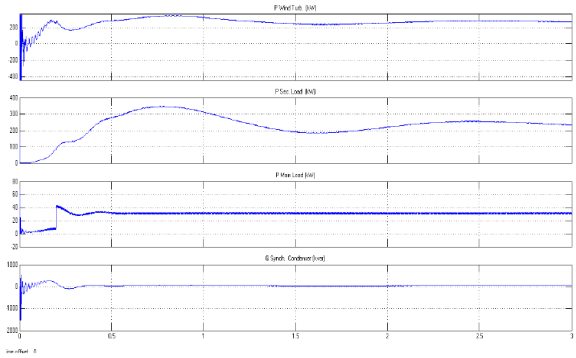

Figure 8. Wind based PMSG output parameters

Simulation results for the proposed structure for step changes in wind speed from 3 to 4 and 4 to 5 m/s. AC voltages and current

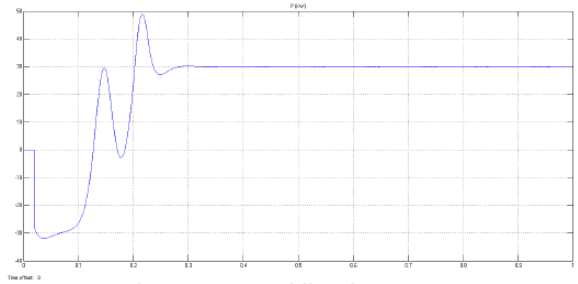

Figure 9. Out Power delivered to Inverter

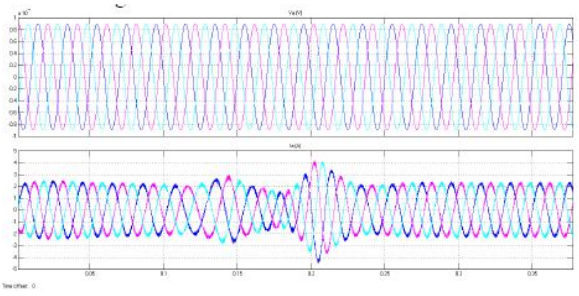

Figure 8. Inverter output voltages and currents

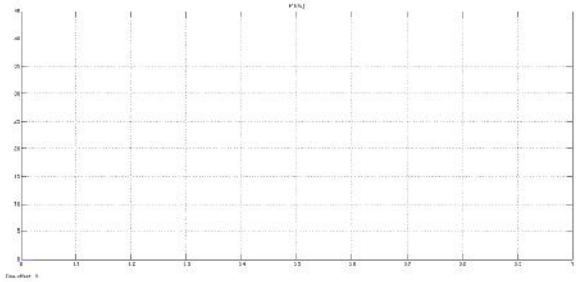

Figure 10. Load Power

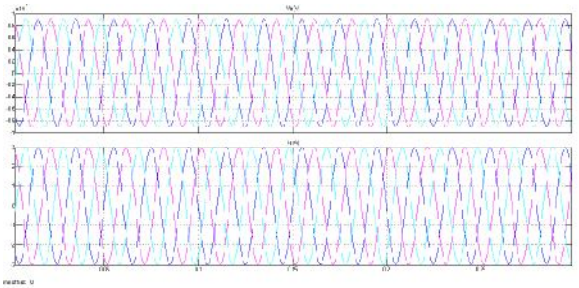

Figure 11. Load Voltages and currents

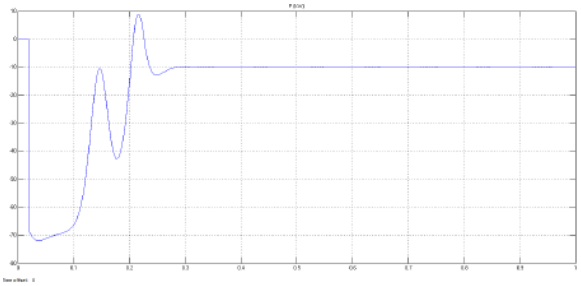

Figure 12. Grid Power

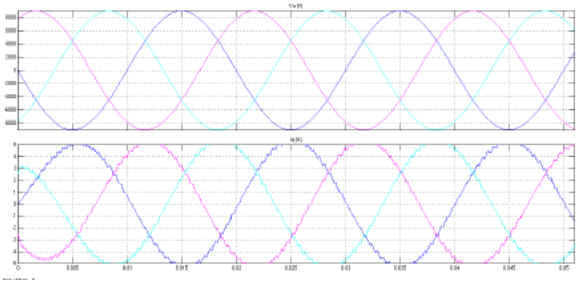

Figure 13. GRID VOLTAGE AND CURRENT

REFERENCES

[1] A. D. Sahin, "Progress and recent trends in wind energy," Progress in Energy Combustion Sci., vol. 30, no. 5, pp. 501–543, 2002.

[2] R. D. Richardson and G. M. Mcnerney, "Wind energy systems," Proc. IEEE, vol. 81, no. 3, pp. 378–389, Mar. 1993.

[3] R. Saidur, M. R. Islam, N. A. Rahim, and K. H. Solangi, "A review on global wind energy policy," Renewable Sustainable Energy Rev., vol. 14, no. 7, pp. 1744–1762, Sep. 2010.

[4] M. T. Ameli, S. Moslehpur, and A. Mirzale, "Feasibility study for replac- ing asynchronous genrators with synchronous generators in wind farm power stations," in Proc. IAJC – IJME, Int. Conf. Eng. Technol., Music City Sheraton, Nashville, TN, US, ENT paper 129Nov. 17–19, 2008.

[5] G. K. Singh, "Self excited generator research—A survey," Electric Power Syst. Res., vol. 69, no. 2/3, pp. 107–114, 2002.

[6] R. C. Bansal, "Three-phase self-excited induction generators: An overview," IEEE Trans. Energy Convers., vol. 20, no. 2, pp. 292–299, Jun. 2005.

[7] S. C. Tripathy, M. Kalantar, and N. D. Rao, "Wind turbine driven self excited induction generator," Energy Convers. Manag., vol. 34, no. 8, pp. 641–648, 1993.

[8] A. Chakraborty, "Advancements in power electronics and drives in inter- face with growing renewable energy resources," Renewable Sustainable Energy Rev., vol. 15, no. 4, pp. 1816–1827, May 2012.

[9] F. D. Gonz´ alez, A. Sumper, O. G. Bellmunt, and R. V. Robles, "A review of energy storage technologies for wind power applications," Renewable Sustainable Energy Rev., vol. 16, no. 4, pp. 2154–2171, May 2012.

[10] N. S. Hasan, M. Y. Hassan, M. S. Majid, and H. A. Rahman, "Review of storage schemes for wind energy systems, "Renewable Sustainable Energy Rev., vol. 21, pp. 237–247, May 2013.

[11] A. M. D. Broe, S. Drouilhet, and V. Gevorgian, "A peak power tracker for small wind turbines in battery charging applications, "IEEETrans.EnergyConvers., vol. 14, no. 4, pp. 1630–1635, Dec. 1999.

[12] R. Kot, M. Rolak, and M. Malinowski, "Comparison of maximum peak power tracking algorithms for a small wind turbine," Math. Comput. Simul., vol. 91, pp. 29–40, 2013.

[13] M. Narayana, G. A. Putrus, M. Jovanovic, P. S. Leung, and S. McDonald, "Generic maximum power point tracking controller for small-scale wind turbines," Renewable Energy, vol. 44, pp. 72–79, Aug. 2012.

★★★